Is the Fornax galaxy cluster hiding its radio sources?

Alvina On 溫薏蓮 (NCTS/NTHU) in collaboration with
Jennifer Chan (Oberlin), Paul Lai (UCL), Kinwah Wu (UCL), Jia-Rou Liou (NTHU),
Hsiang-Yi Karen Yang (NTHU/NCTS) and John ZuHone (CfA)

alvina.on@phys.ncts.ntu.edu.tw

The Northern lights – also known as the aurora borealis – dancing across the night sky in Alaska.

Background credit: The National Geographic's Short Film Showcase by Alexis Coram

The Fornax cluster – optical

Credit: Mikel Martinez 2020

The Fornax cluster – optical

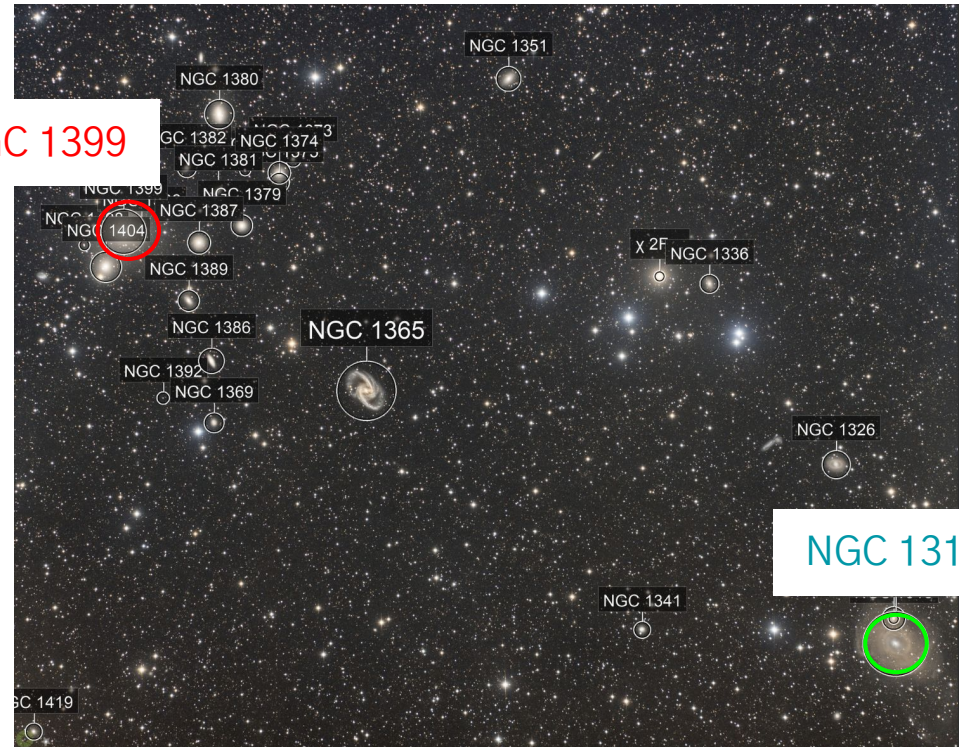

Credit: Mikel Martinez 2020

- nearby, $z \approx 0.0046$
- ~ 390 member galaxies
- low total ~ 10^{13} solar masses
- cD-type central galaxy NGC 1399
- Fornax A: NGC 1316
- core: early-type galaxies – virialised and well-evolved?

The Fornax cluster – optical

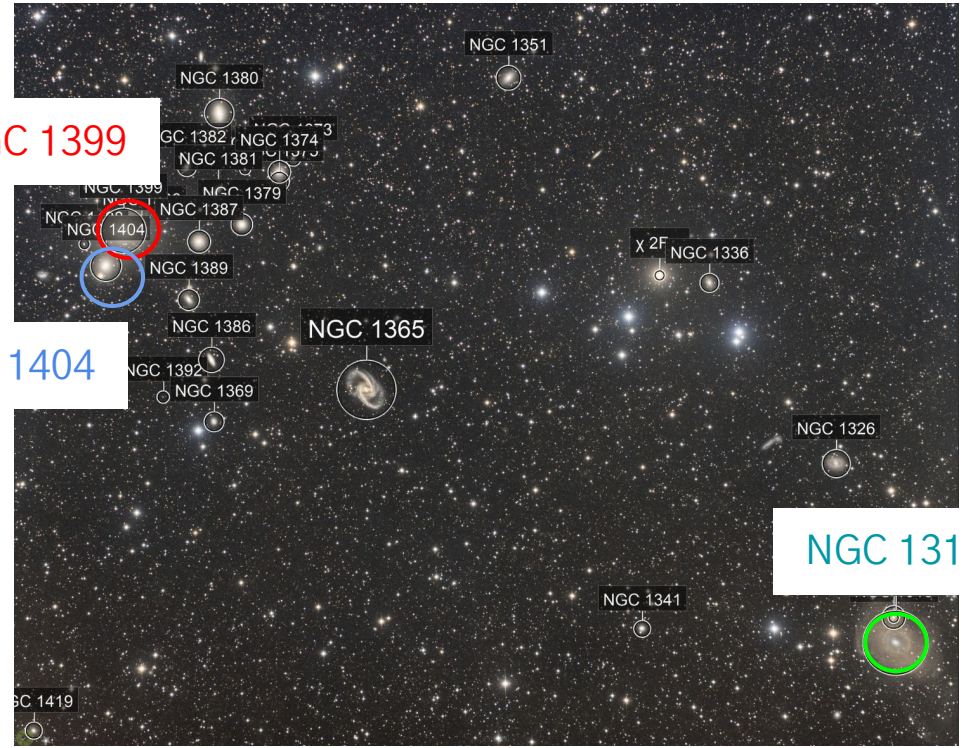

Credit: Mikel Martinez 2020

- nearby, $z \approx 0.0046$
- ~ 390 member galaxies
- low total ~ 10^{13} solar masses
- cD-type central galaxy NGC 1399
- Fornax A: NGC 1316
- core: early-type galaxies – virialised and well-evolved?

However, recent studies indicated that the cluster is still assembling mass through a series of ongoing mergers:

NGC 1399 + NGC 1316

NGC 1399 + in-falling NGC 1404

The Fornax cluster – radio linear polarised intensity

central galaxy NGC 1399

fan-like beam artefacts

beamforming errors around Fornax A

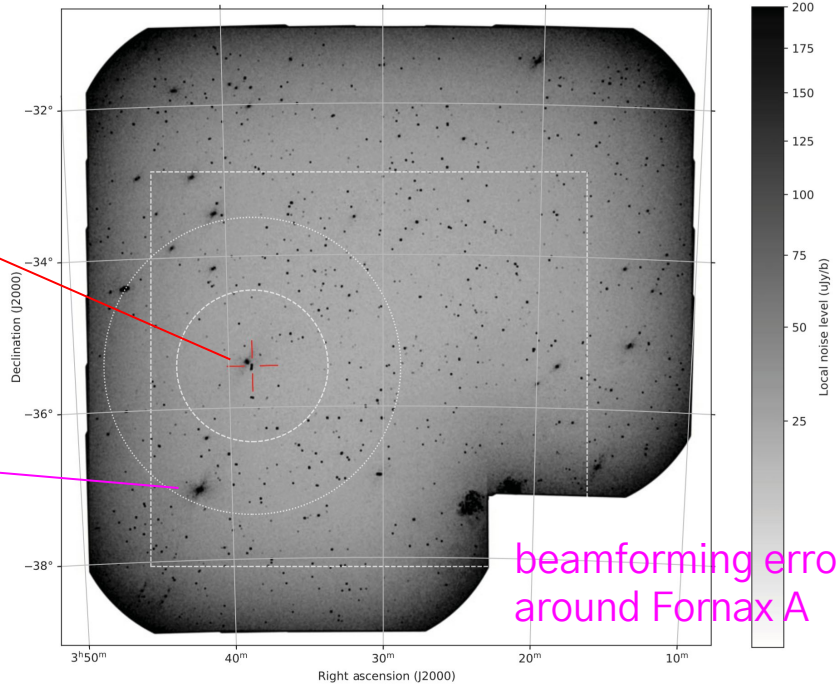

Figure 3. The local root-mean-squared (RMS) noise in the peak-*P* map. This is supplied in lieu of the peak-*P* map itself, which renders point sources effectively invisible for our high-resolution, large area map. This RMS map was generated by running a square sliding window of width and height both equal to five synthesised beamwidths over the peak-*P* map and calculating the RMS values of the pixels inside the window. The image shown here has a square root stretch applied. Linearly polarised radio sources are visible as a marked increase in the local RMS value. In source-free regions, the RMS is typically ∼30 μJy beam^{-1}, except at the mosaic edges, and in the vicinity of bright sources, where the faint imprint of the synthesised beam manifests as narrow, diagonal fan-like structures. The centre of the Fornax cluster is indicated with a red cross-hair. Fornax A is partially visible in the bottom-right corner of the map, where six beams are missing due to beamforming errors. The white dashed box approximately indicates the region shown in Figure 8. The white dashed line indicates an angular radius of 1°, while the white dotted line indicates the 705 kpc (1.96°) virial radius of the cluster.

- ASKAP POSSUM survey
- "polarised intensity" map 747 – 1027 MHz
- ~ 25 RMs per square degree
- ~ 870 linearly polarised **background** sources (black dots) with a median fractional polarisation 4.8%
- white box: analysis region
- inner circle: 1-degree angular radius
- outer circle: 705 kpc virial radius of cluster

(Anderson+ 2021)

The Fornax cluster – “missing” polarised sources?

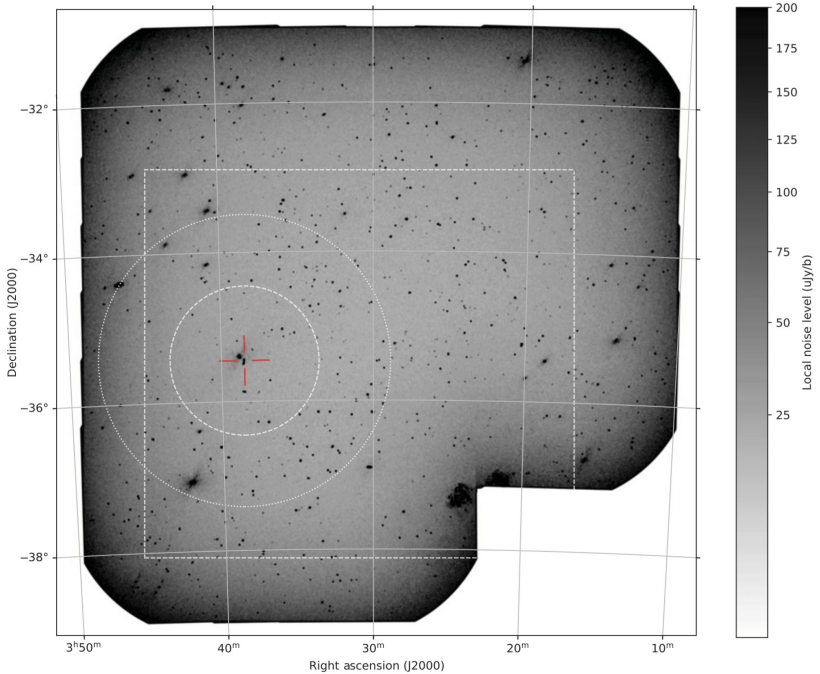

Figure 3. The local root-mean-squared (RMS) noise in the peak-*P* map. This is supplied in lieu of the peak-*P* map itself, which renders point sources effectively invisible for our high-resolution, large area map. This RMS map was generated by running a square sliding window of width and height both equal to five synthesised beamwidths over the peak-*P* map and calculating the RMS values of the pixels inside the window. The image shown here has a square root stretch applied. Linearly polarised radio sources are visible as a marked increase in the local RMS value. In source-free regions, the RMS is typically $\sim$30 μJy beam^{-1}, except at the mosaic edges, and in the vicinity of bright sources, where the faint imprint of the synthesised beam manifests as narrow, diagonal fan-like structures. The centre of the Fornax cluster is indicated with a red cross-hair. Fornax A is partially visible in the bottom-right corner of the map, where six beams are missing due to beamforming errors. The white dashed box approximately indicates the region shown in Figure 8. The white dashed line indicates an angular radius of 1°, while the white dotted line indicates the 705 kpc (1.96°) virial radius of the cluster.

(Anderson+ 2021)

The Fornax cluster – “missing” polarised sources?

empty “patches” by eye

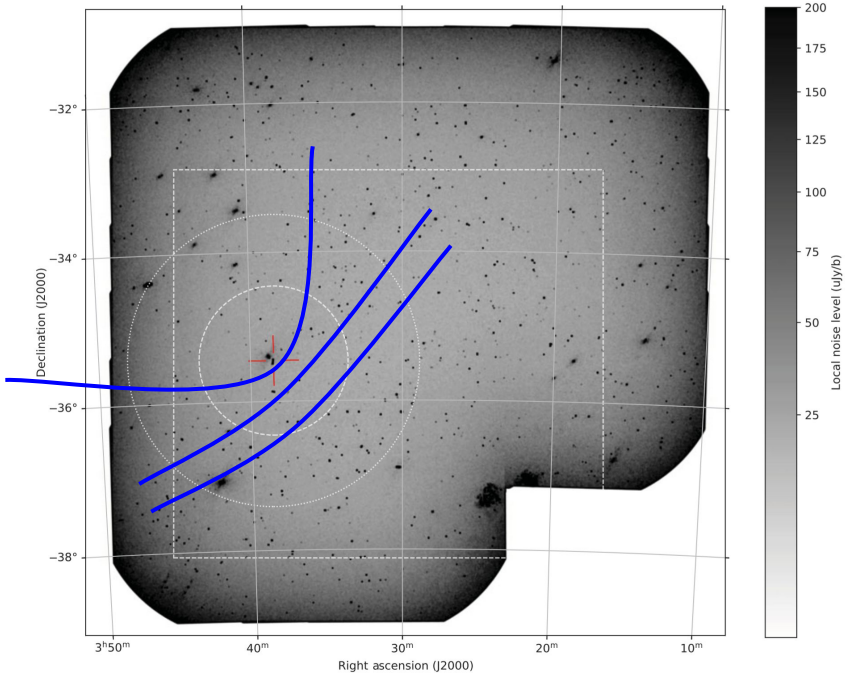

Figure 3. The local root-mean-squared (RMS) noise in the peak-*P* map. This is supplied in lieu of the peak-*P* map itself, which renders point sources effectively invisible for our high-resolution, large area map. This RMS map was generated by running a square sliding window of width and height both equal to five synthesised beamwidths over the peak-*P* map and calculating the RMS values of the pixels inside the window. The image shown here has a square root stretch applied. Linearly polarised radio sources are visible as a marked increase in the local RMS value. In source-free regions, the RMS is typically ∼30 μJy beam^{-1}, except at the mosaic edges, and in the vicinity of bright sources, where the faint imprint of the synthesised beam manifests as narrow, diagonal fan-like structures. The centre of the Fornax cluster is indicated with a red cross-hair. Fornax A is partially visible in the bottom-right corner of the map, where six beams are missing due to beamforming errors. The white dashed box approximately indicates the region shown in Figure 8. The white dashed line indicates an angular radius of 1°, while the white dotted line indicates the 705 kpc (1.96°) virial radius of the cluster.

(Anderson+ 2021)

Faraday rotation – schematic

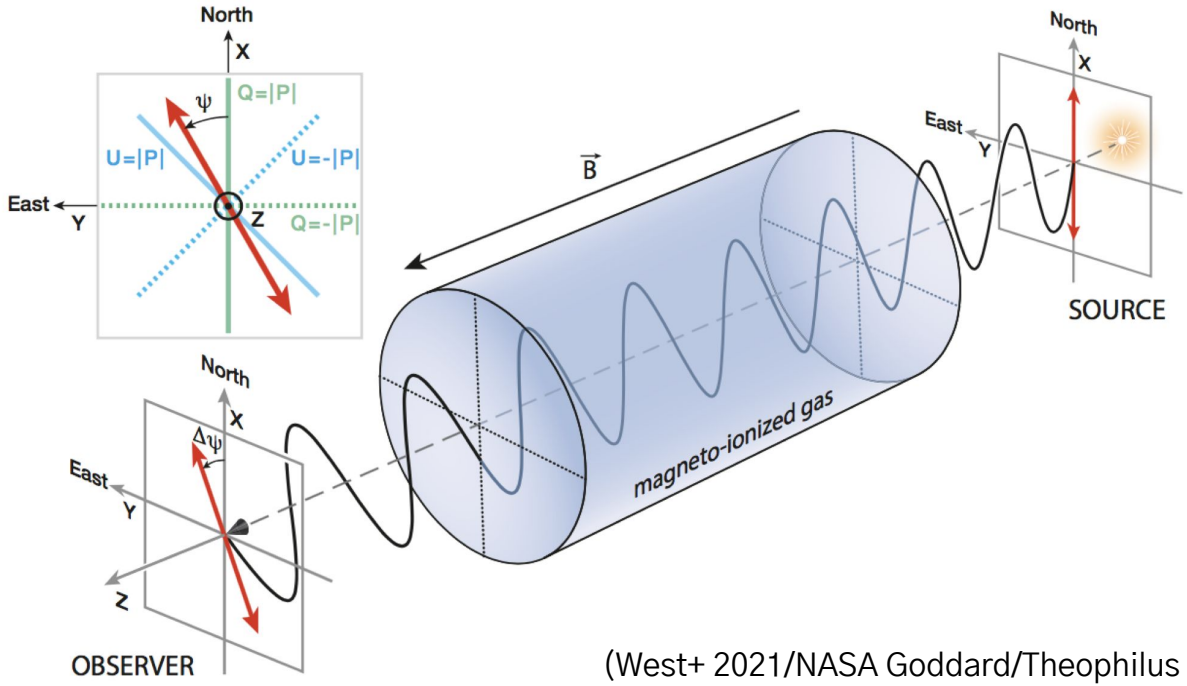

(West+ 2021/NASA Goddard/Theophilus Britt Griswold)

Measuring the invisible

Faraday rotation measure (RM) at radio wavelengths is commonly used to diagnose large-scale magnetic fields.

rotation measure

observed wavelength

$$\mathcal{R} = (\Delta\varphi)\lambda^{-2} = (\varphi - \varphi_0)\lambda^{-2}$$

observed polarisation angle

intrinsic polarisation angle

Rotation measure (RM)

In the context of polarised radiative transfer

distance between the source and the observer

$$\mathcal{R}(s) = 0.812 \int_{s_0}^{s} \frac{\mathrm{d}s'}{\mathrm{pc}} \left(\frac{n_{\mathrm{e,\,th}}(s')}{\mathrm{cm}^{-3}} \right) \left(\frac{B_{\parallel}(s')}{\mu\mathrm{G}} \right) \mathrm{rad\ m}^{-2}$$

thermal electron number density

B-field strength along line-of-sight

assuming:

no absorption, no synchrotron emission, no Faraday conversion

only thermal electrons are present

Beyond galactic scales – Coma cluster

Magnetic fields are relatively weaker and more difficult to be observed

radio synchrotron emission and Faraday rotation measures as probes

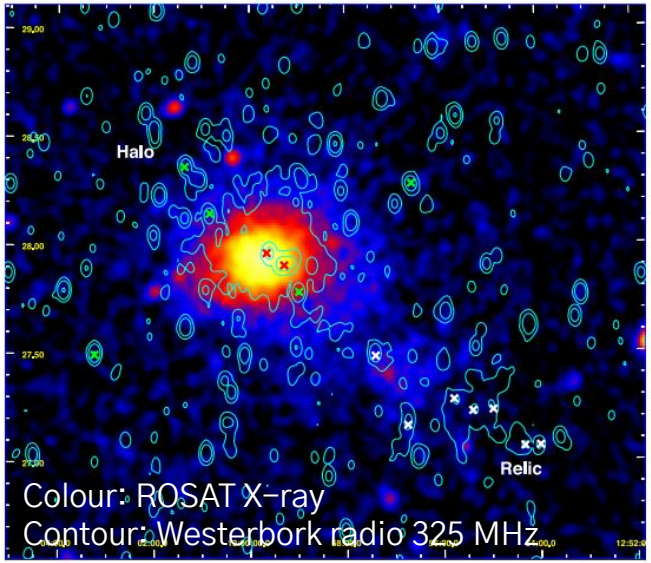

Coma cluster and NGC 4839 group

Colour: RM Contour: total radio intensity 1.4 GHz

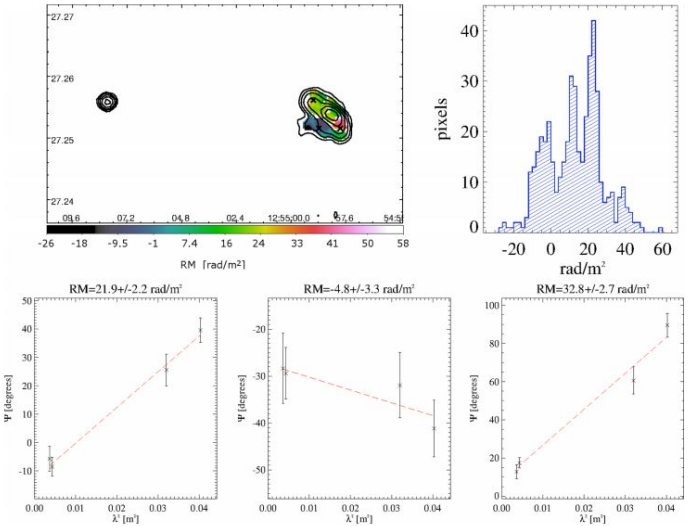

(Bonafede+ 2013)

The Fornax cluster – “missing” polarised sources?

empty “patches” by eye

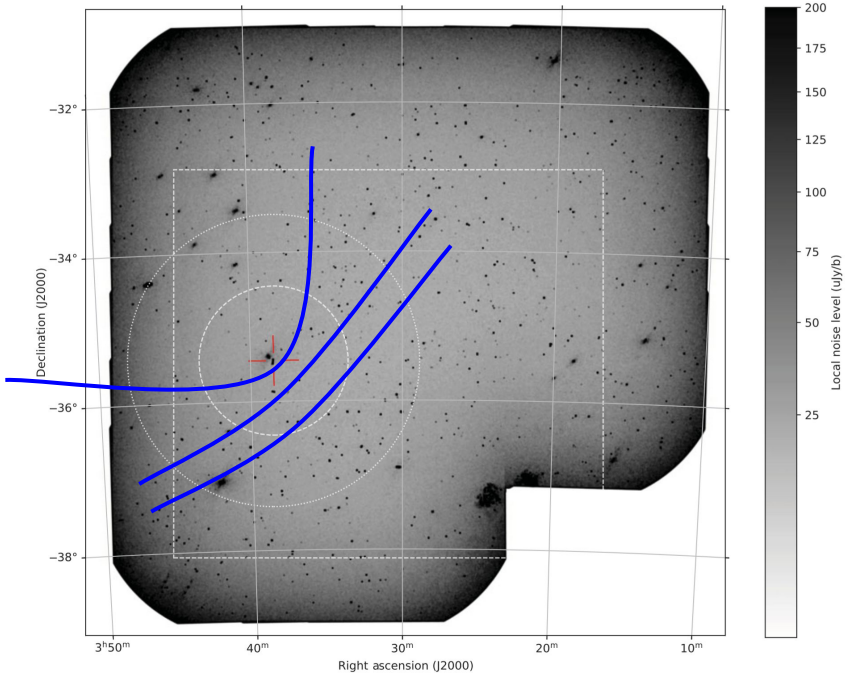

Figure 3. The local root-mean-squared (RMS) noise in the peak-*P* map. This is supplied in lieu of the peak-*P* map itself, which renders point sources effectively invisible for our high-resolution, large area map. This RMS map was generated by running a square sliding window of width and height both equal to five synthesised beamwidths over the peak-*P* map and calculating the RMS values of the pixels inside the window. The image shown here has a square root stretch applied. Linearly polarised radio sources are visible as a marked increase in the local RMS value. In source-free regions, the RMS is typically ∼30 μJy beam^{-1}, except at the mosaic edges, and in the vicinity of bright sources, where the faint imprint of the synthesised beam manifests as narrow, diagonal fan-like structures. The centre of the Fornax cluster is indicated with a red cross-hair. Fornax A is partially visible in the bottom-right corner of the map, where six beams are missing due to beamforming errors. The white dashed box approximately indicates the region shown in Figure 8. The white dashed line indicates an angular radius of 1°, while the white dotted line indicates the 705 kpc (1.96°) virial radius of the cluster.

(Anderson+ 2021)

The Fornax cluster – X-ray and RM observations

contours: X-rays
cyan: Chandra (0.3 – 1.5 keV)
magenta: ROSAT (1 – 2.4 keV)

colours: RMs
(anything < 200 rad^2 m^{-4} masked as black)

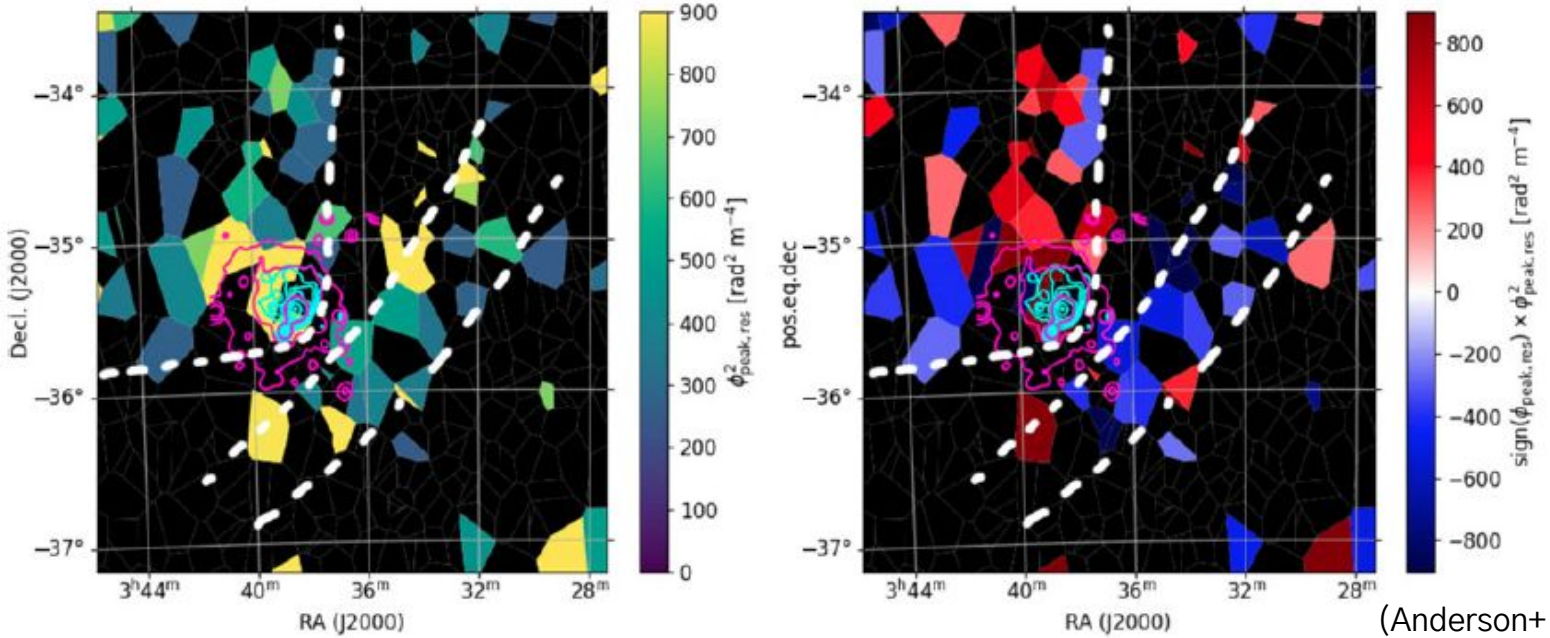

(Anderson+ 2021)

Is there truly a deficit of polarised sources?

Is there truly a deficit of polarised sources?

Yes

Comparing the RM grids – MeerKAT vs ASKAP surveys

contours: X-rays
e-ROSITA (0.2 – 2.3 keV)
extended radio sources included

colours: RMs (< 200 rad^2 m^{-4} masked as black)
cyan: Chandra (0.3 – 1.5 keV)
magenta: ROSAT (1 – 2.4 keV)

New

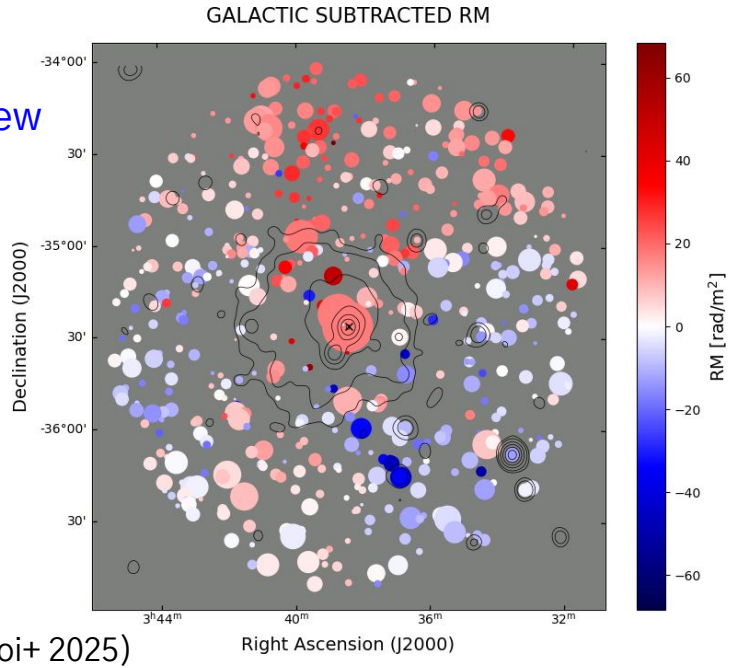

(Loi+ 2025)

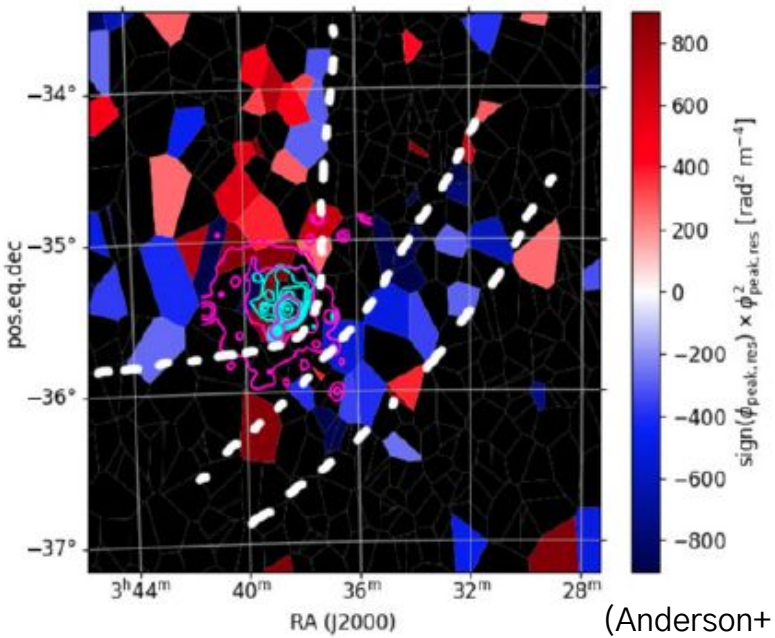

(Anderson+ 2021)

Comparing the RM grids – MeerKAT vs ASKAP surveys

contours: X-rays
e-ROSITA (0.2 – 2.3 keV)
extended radio sources included

colours: RMs (< 200 rad^2 m^{-4} masked as black)
cyan: Chandra (0.3 – 1.5 keV)
magenta: ROSAT (1 – 2.4 keV)

New

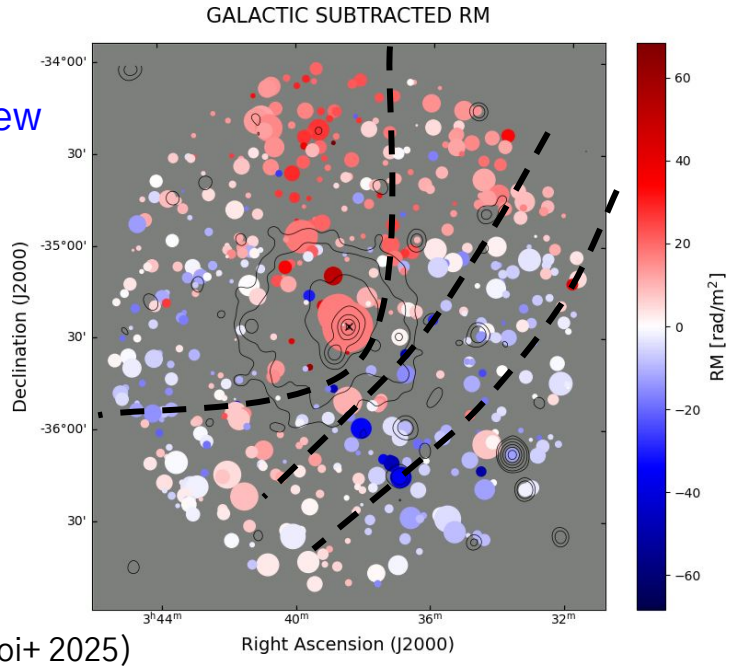

(Loi+ 2025)

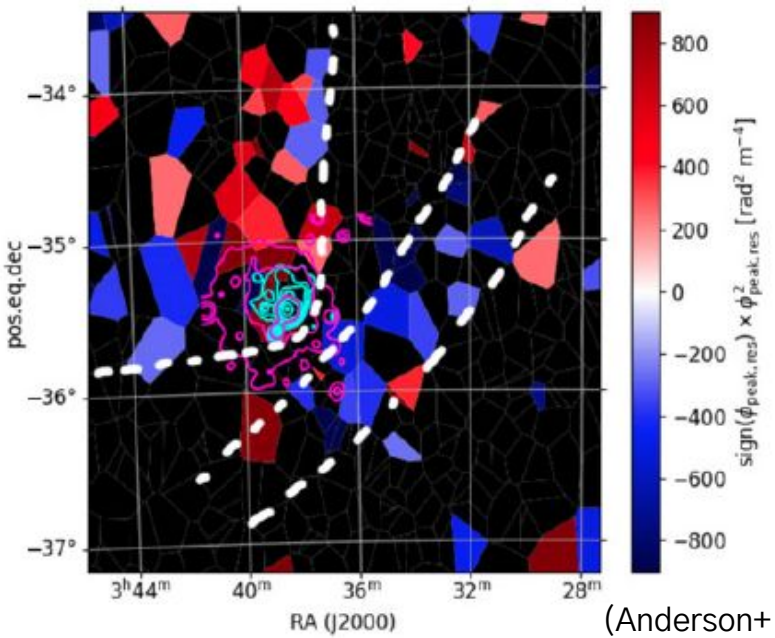

(Anderson+ 2021)

Possible scenarios for Mpc-scale depolarisation

shock passage

sloshing motion

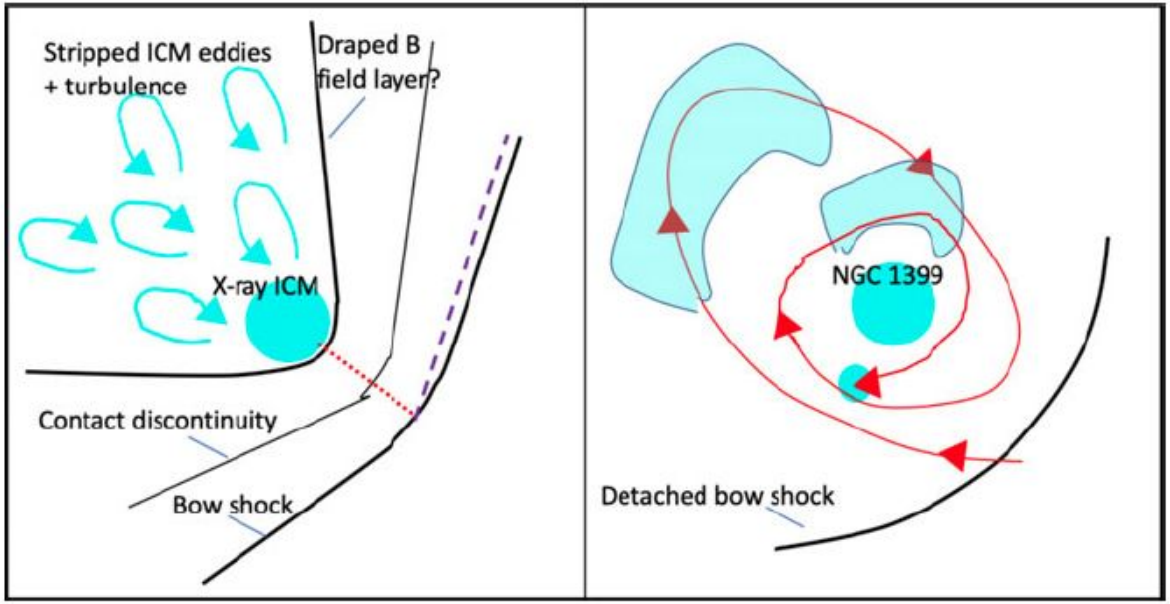

(Anderson+ 2021)

Building a conic shock model

the large-scale shock compresses the gas and amplifies the magnetic field

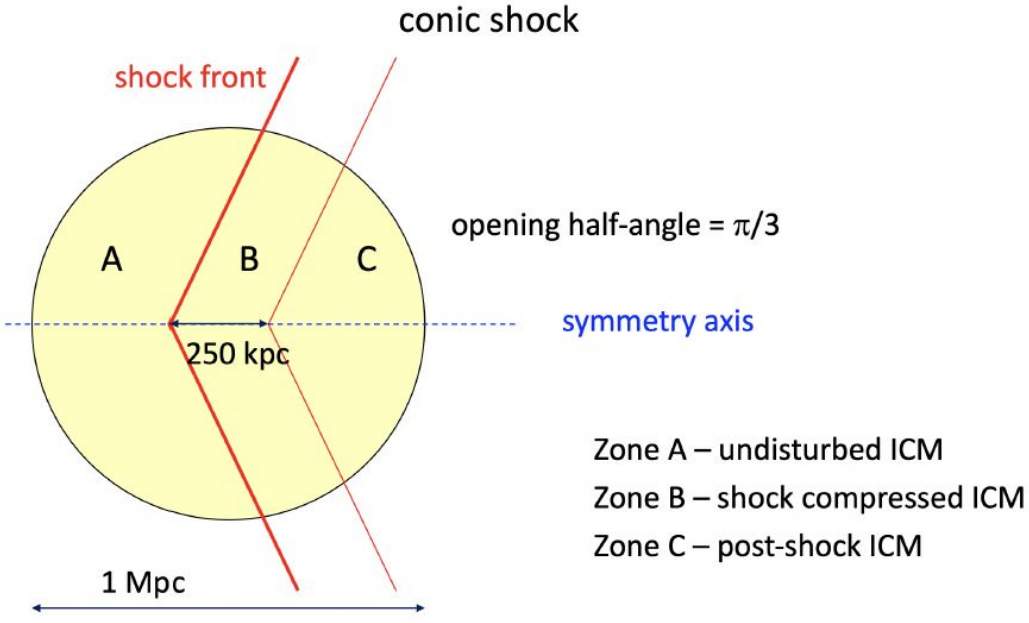

thermal electron number density follows a beta model

B-field strength in B is twice of A

A and C have the same number of thermal electrons

C has twice the number of non-thermal electrons than A

cluster temperature 10^7 K

(**On,** Chan, Lai and Wu, MNRAS, under review)

Synthetic radio maps of our shock model at 0°

full polarised radiative transfer calculations of 1024 background point sources

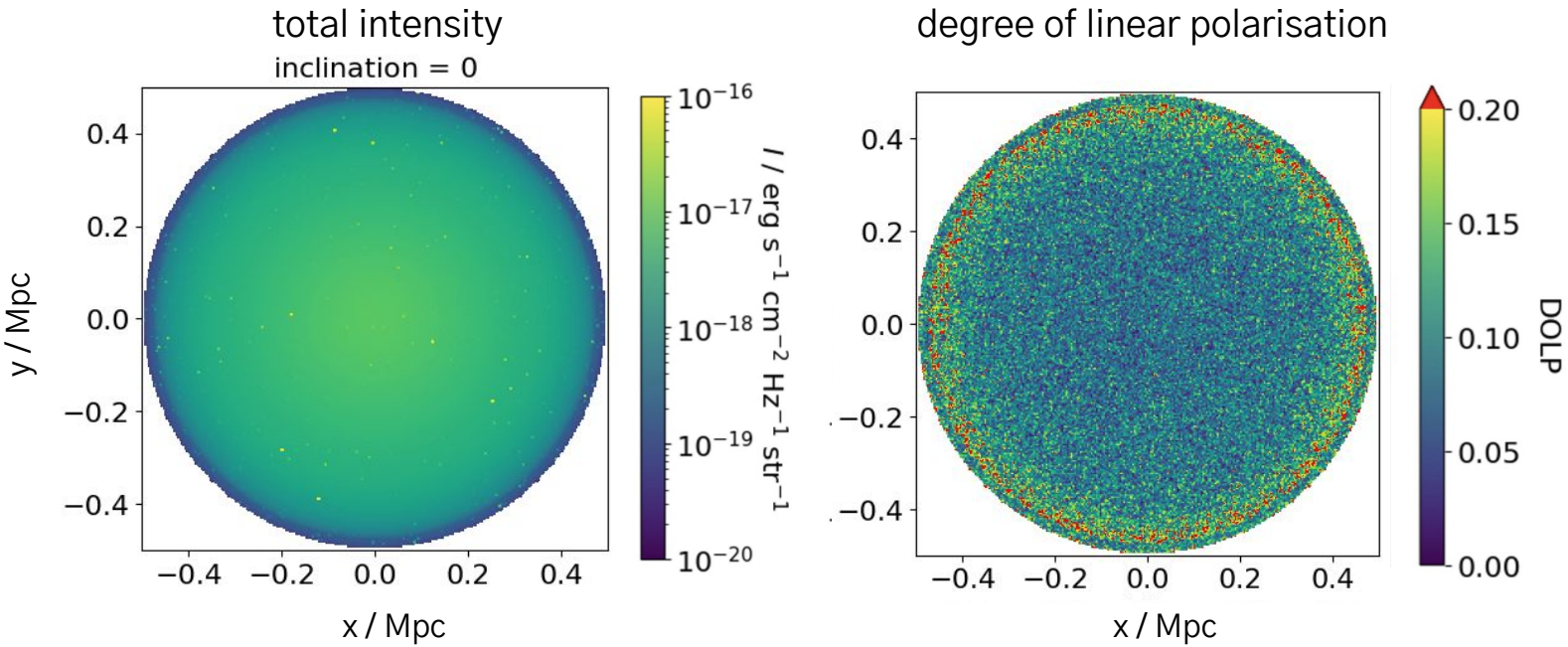

(**On,** Chan, Lai and Wu, MNRAS, under review)

Synthetic radio maps of our shock model at 60°

full polarised radiative transfer calculations of 1024 background point sources

total intensity

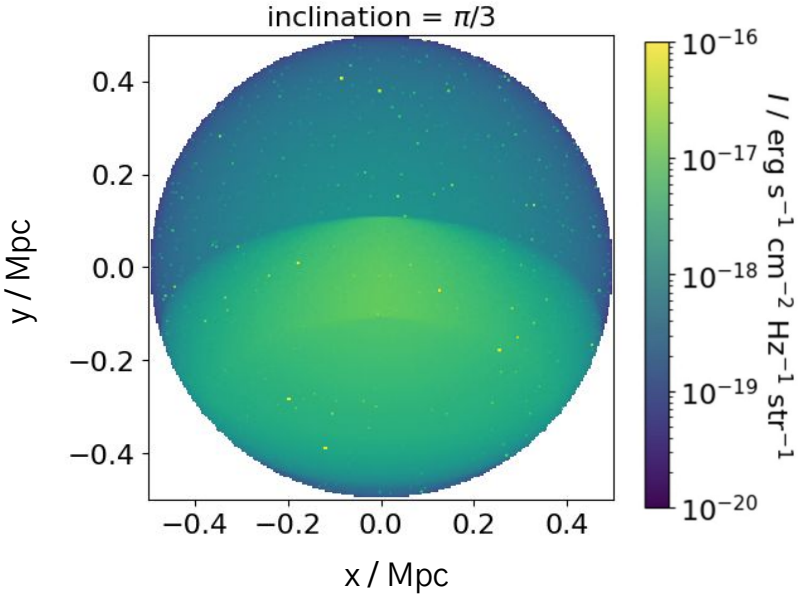

degree of linear polarisation

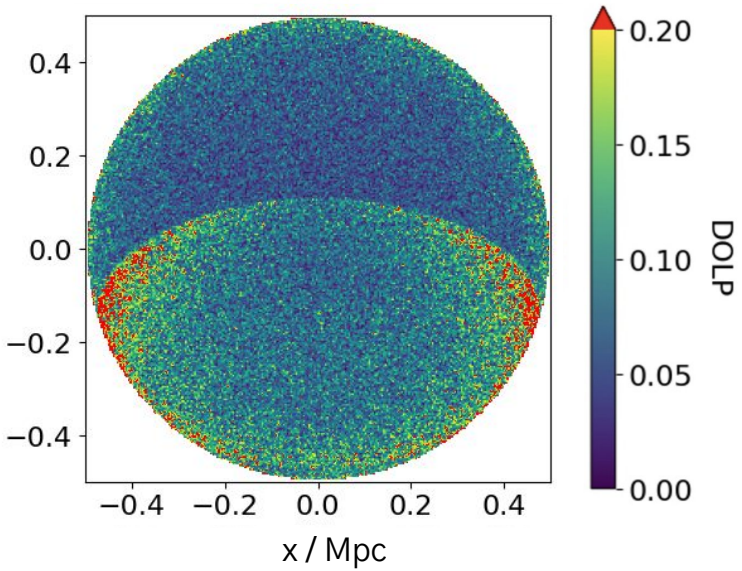

(**On,** Chan, Lai and Wu, MNRAS, under review)

Synthetic radio maps of our shock model at 90°

full polarised radiative transfer calculations of 1024 background point sources

total intensity

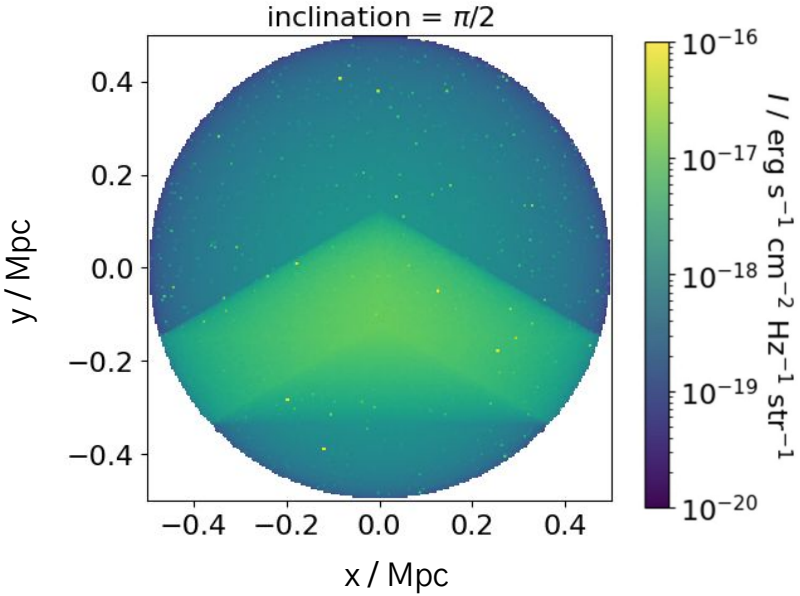

degree of linear polarisation

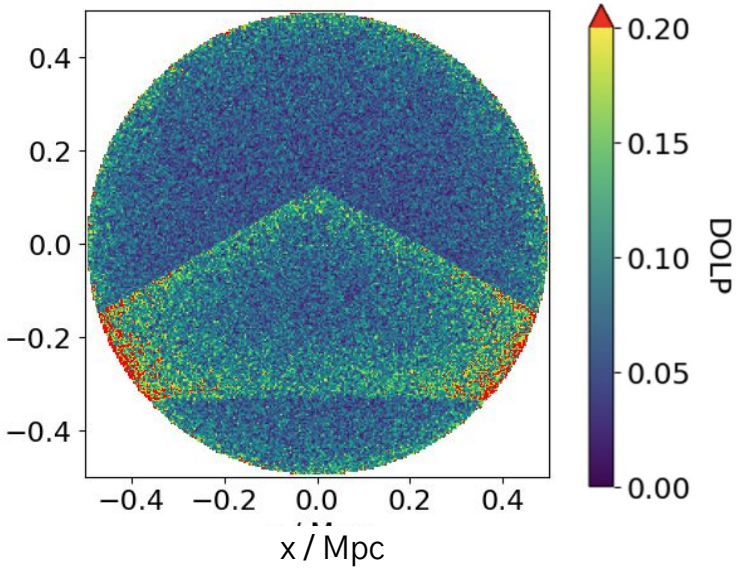

(**On,** Chan, Lai and Wu, MNRAS, under review)

Synthetic radio maps of our shock model at 90°

full polarised radiative transfer calculations of 1024 background point sources

total intensity

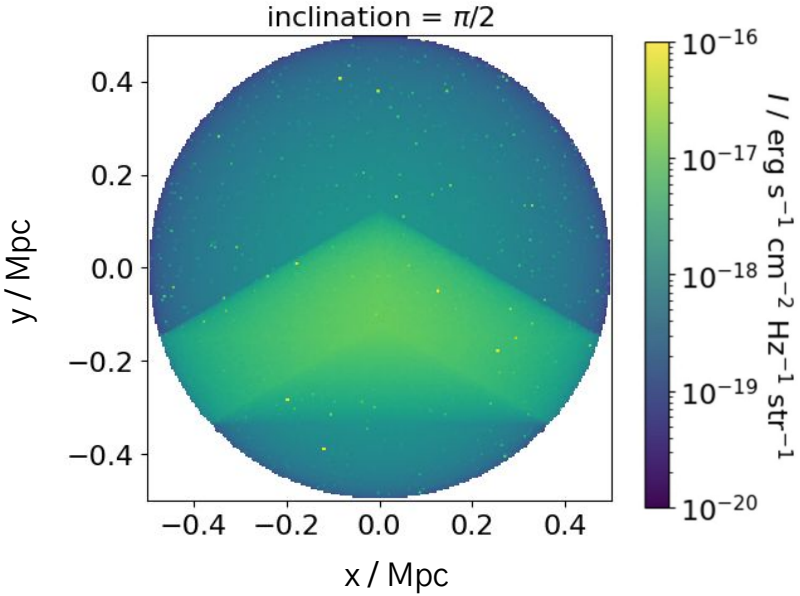

degree of linear polarisation

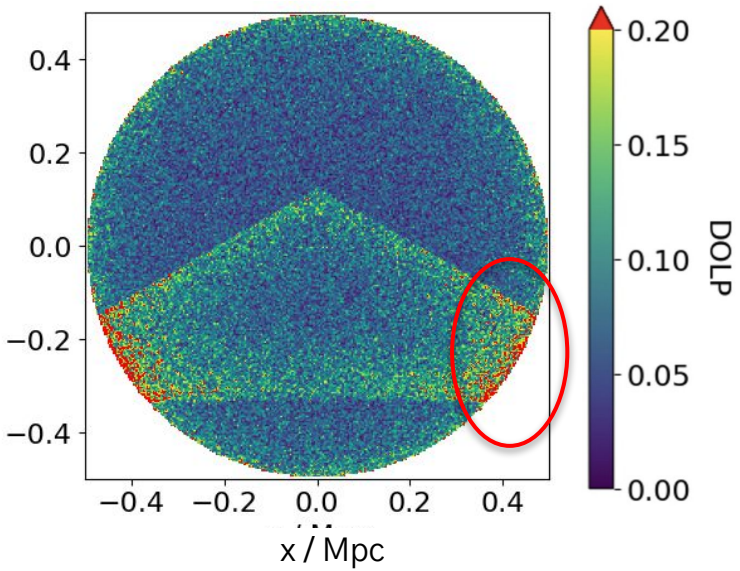

(**On,** Chan, Lai and Wu, MNRAS, under review)

Larger fraction of point sources being enhanced

many point sources are initially fainter or comparable to the diffuse ICM

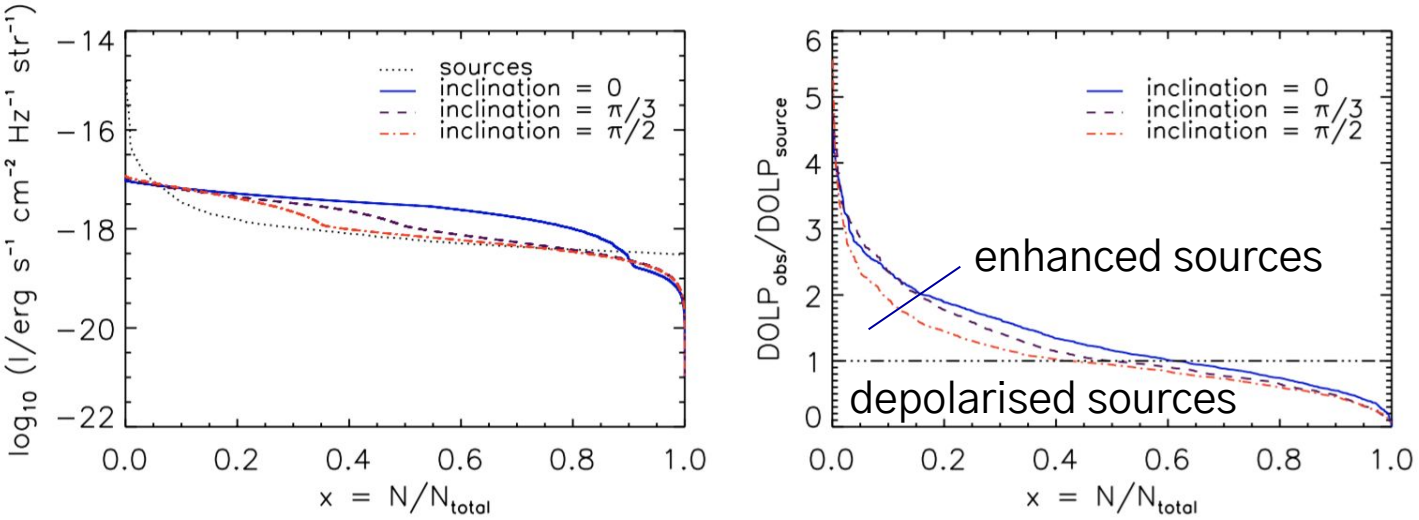

Figure 7. *Left*: The ranked distributions for Stokes total intensity I of the background point sources (black dotted line) and of the diffuse ICM for a galaxy cluster containing a large-scale shock (see Figure 6), viewed at three different inclination angles 0 (blue solid line), $\pi/3$ (violet dashed line) and $\pi/2$ radian (red dash-dot line). *Right*: The corresponding ranked distributions for the ratio between the observed DOLP and the source DOLP.

(**On,** Chan, Lai and Wu, MNRAS, under review)

the intracluster shock has a larger degree of linear polarisation than the sources and the ambient medium

the intracluster shock has a larger degree of linear polarisation than the sources and the ambient medium

one of the essential conditions for polarisation enhancement to occur

Scatter of observed DOLP vs. total intensity *I* at 0°

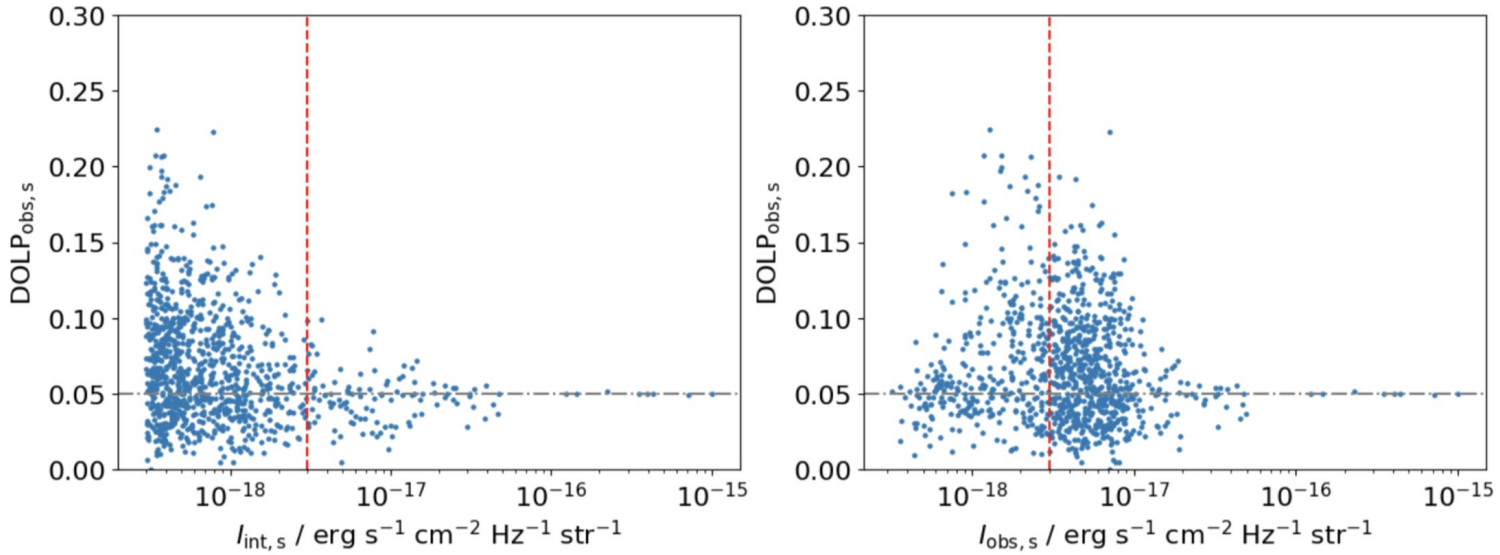

Figure 8. The scatter of the observed DOLP of each background point source in the intracluster shock model plotted against its intrinsic total intensity (left column) and its observed total intensity (right column) viewed at 0 (top row), $\pi/3$ (middle row) and $\pi/2$ (bottom row) radian. From the top row, the vertical red dashed line marks the median total intensity of the diffuse medium at $I_m = 3.03 \times 10^{-18}$, 1.13×10^{-18}, and 7.47×10^{-19} erg s^{-1} cm^{-2} Hz^{-1} str^{-1}. There is a higher fraction of enhanced sources at lower inclinations, arising from the larger projected filling factor of the shock, whereas at higher inclinations, more point sources become depolarised due to LOS field cancellations in the ambient medium.

(**On,** Chan, Lai and Wu, MNRAS, under review)

Scatter of observed DOLP vs. total intensity I at 60°

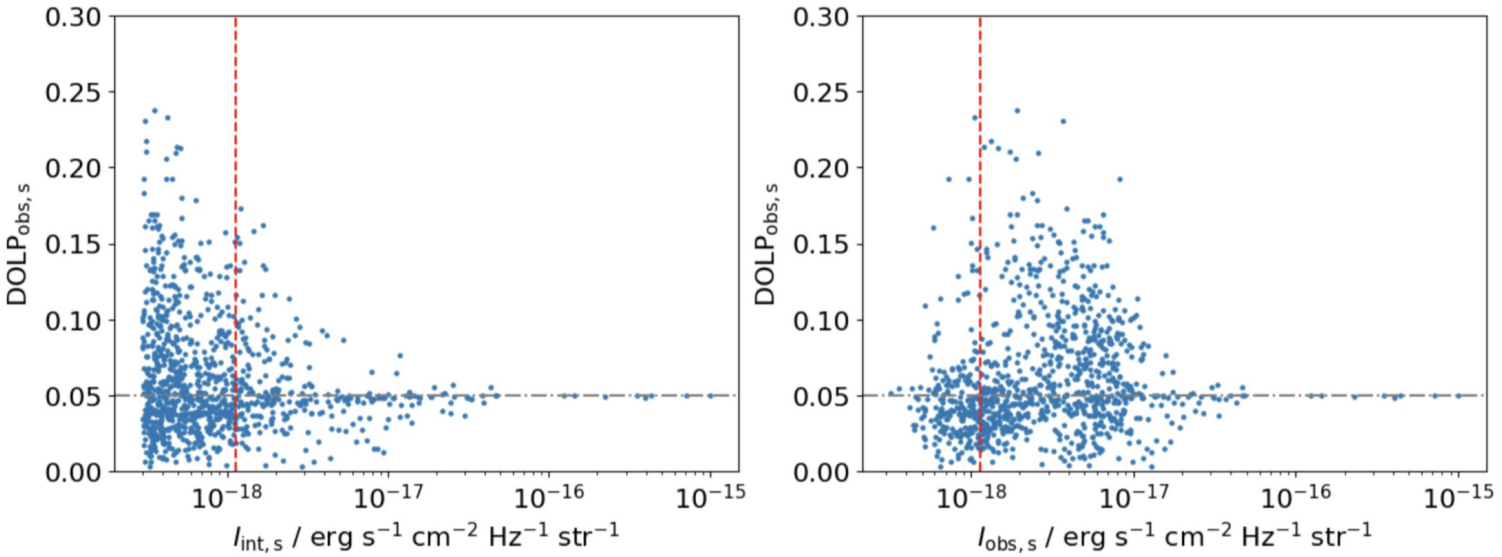

Figure 8. The scatter of the observed DOLP of each background point source in the intracluster shock model plotted against its intrinsic total intensity (left column) and its observed total intensity (right column) viewed at 0 (top row), $\pi/3$ (middle row) and $\pi/2$ (bottom row) radian. From the top row, the vertical red dashed line marks the median total intensity of the diffuse medium at $I_m = 3.03 \times 10^{-18}$, 1.13×10^{-18}, and 7.47×10^{-19} erg s^{-1} cm^{-2} Hz^{-1} str^{-1}. There is a higher fraction of enhanced sources at lower inclinations, arising from the larger projected filling factor of the shock, whereas at higher inclinations, more point sources become depolarised due to LOS field cancellations in the ambient medium.

(**On,** Chan, Lai and Wu, MNRAS, under review)

Scatter of observed DOLP vs. total intensity *I* at 90°

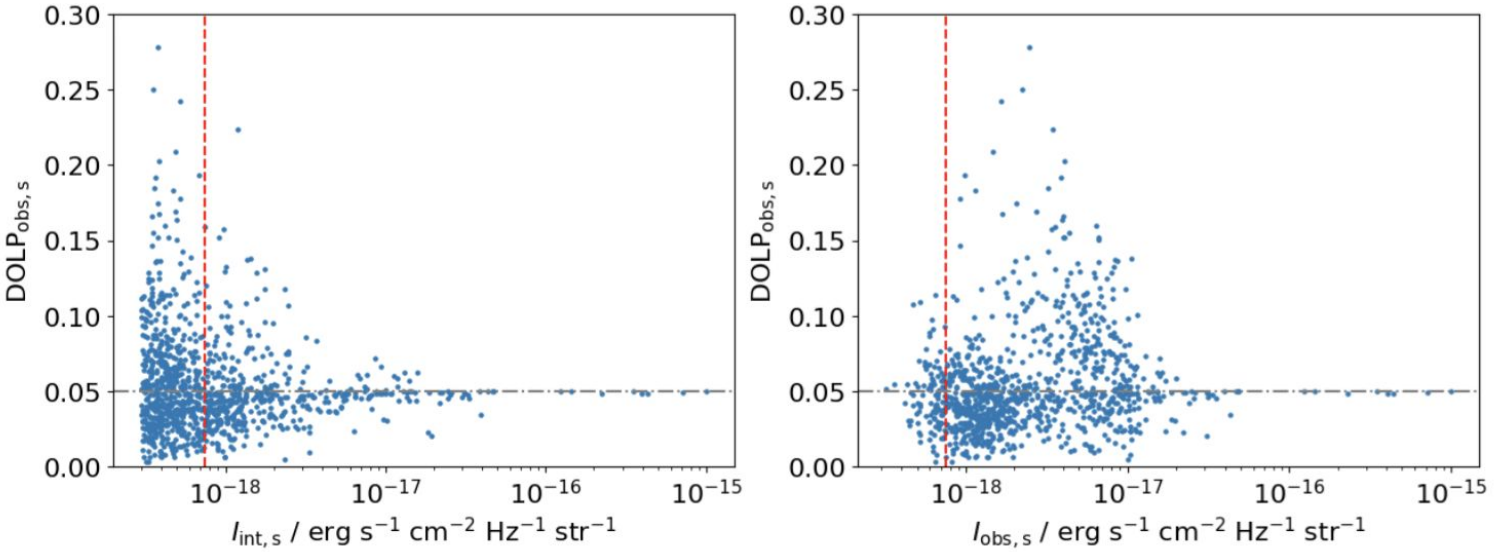

Figure 8. The scatter of the observed DOLP of each background point source in the intracluster shock model plotted against its intrinsic total intensity (left column) and its observed total intensity (right column) viewed at 0 (top row), $\pi/3$ (middle row) and $\pi/2$ (bottom row) radian. From the top row, the vertical red dashed line marks the median total intensity of the diffuse medium at $I_m = 3.03 \times 10^{-18}$, 1.13×10^{-18}, and 7.47×10^{-19} erg s^{-1} cm^{-2} Hz^{-1} str^{-1}. There is a higher fraction of enhanced sources at lower inclinations, arising from the larger projected filling factor of the shock, whereas at higher inclinations, more point sources become depolarised due to LOS field cancellations in the ambient medium.

(**On,** Chan, Lai and Wu, MNRAS, under review)

the observed DOLP of background sources is modulated by the shock orientation and hence its projected filling factor

Changes in polarisation statistics with viewing angle

0°

60°

90°

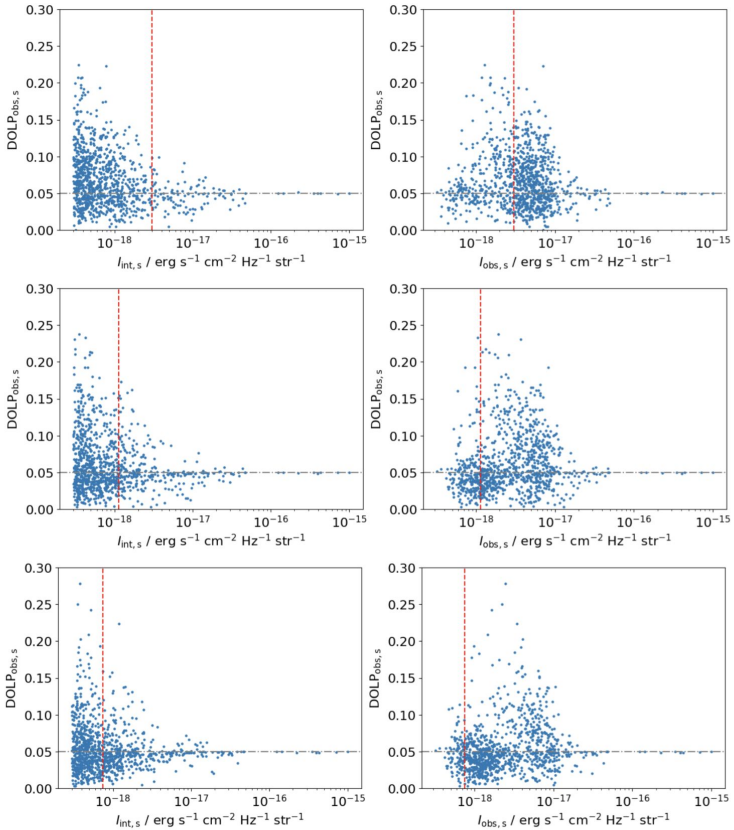

fractional increase in enhanced sources towards lower inclination, arising from the larger projected filling factor of the shock

more point sources are depolarised at higher inclinations due to more line–of–sight cancellations in the ambient medium

red line: median total intensity of the ICM

(**On,** Chan, Lai and Wu, MNRAS, under review)

Not all point sources are created equal

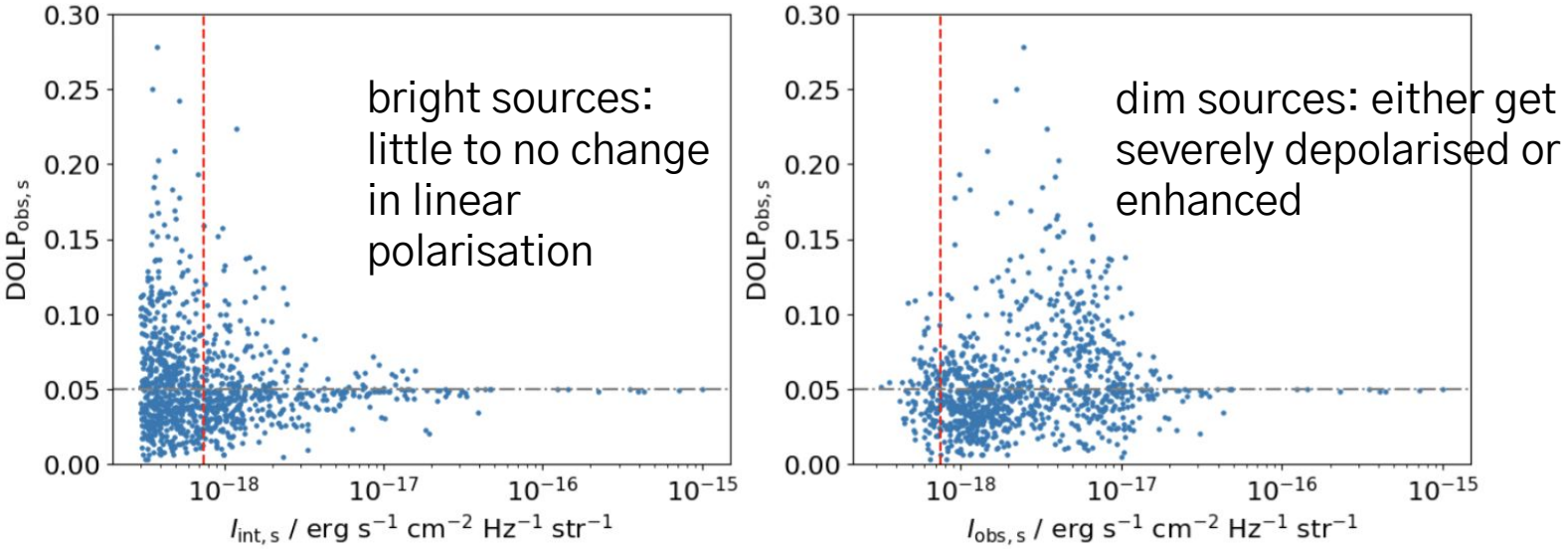

Figure 8. The scatter of the observed DOLP of each background point source in the intracluster shock model plotted against its intrinsic total intensity (left column) and its observed total intensity (right column) viewed at 0 (top row), $\pi/3$ (middle row) and $\pi/2$ (bottom row) radian. From the top row, the vertical red dashed line marks the median total intensity of the diffuse medium at $I_m = 3.03 \times 10^{-18}$, 1.13×10^{-18}, and 7.47×10^{-19} erg s^{-1} cm^{-2} Hz^{-1} str^{-1}. There is a higher fraction of enhanced sources at lower inclinations, arising from the larger projected filling factor of the shock, whereas at higher inclinations, more point sources become depolarised due to LOS field cancellations in the ambient medium.

(**On,** Chan, Lai and Wu, MNRAS, under review)

Carrying out a FLASH MHD cluster merger simulation

5:1 mass ratio, 8 Mpc simulation box
initial tangled B-field, power-law spectrum cutoffs at 43 kpc and 500 kpc
plasma beta = 100

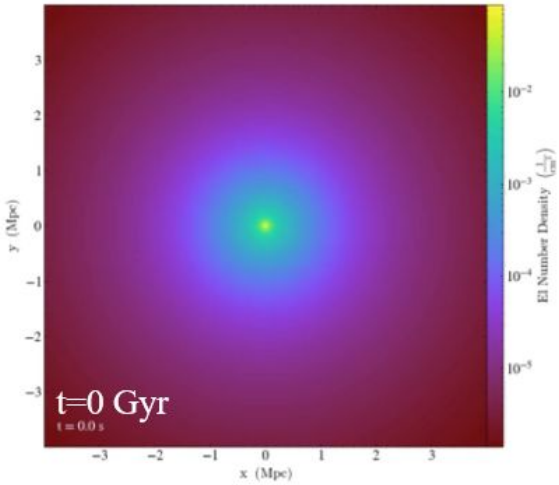

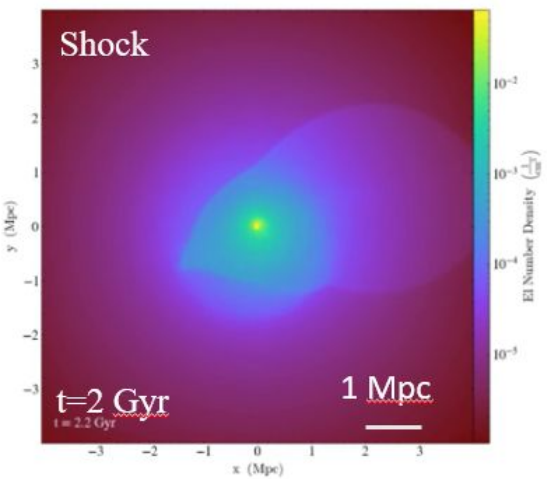

Zoomed in to the Center

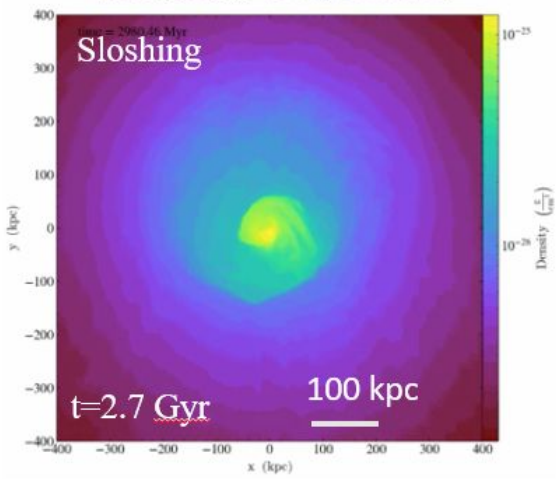

(Liou, **On,** Yang and ZuHone, ApJ, under review)

Polarisation signatures of shock and sloshing cold front

using 3D FLASH MHD simulations of a cluster merger scenario

total radio intensity

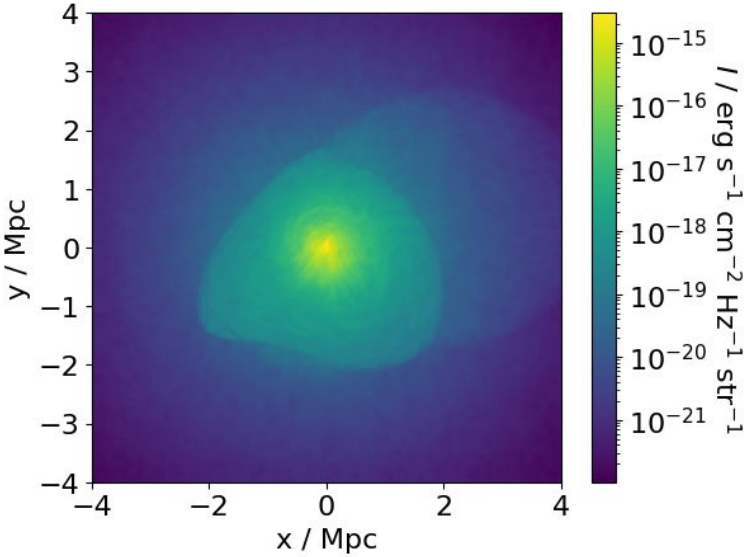

degree of linear polarisation

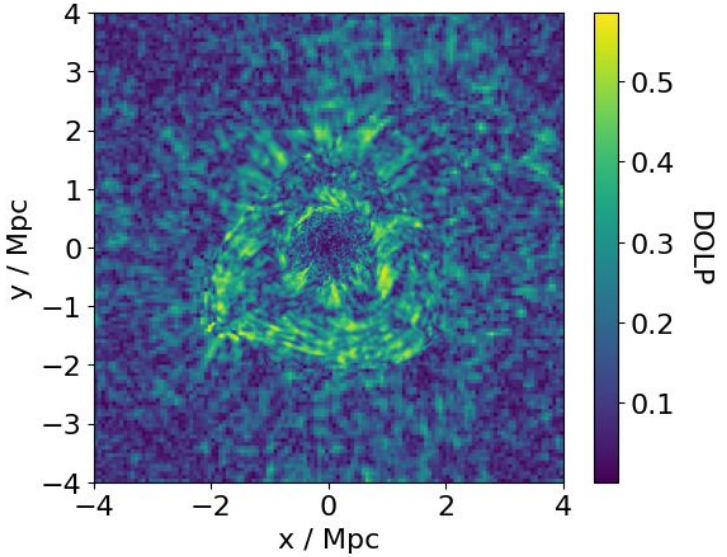

(Liou, **On,** Yang and ZuHone, ApJ, under review)

Enhancement in RMs after a shock passes by

using 3D FLASH MHD simulations of a cluster merger scenario

colours: RM

cyan contours: projected X-ray emission

before

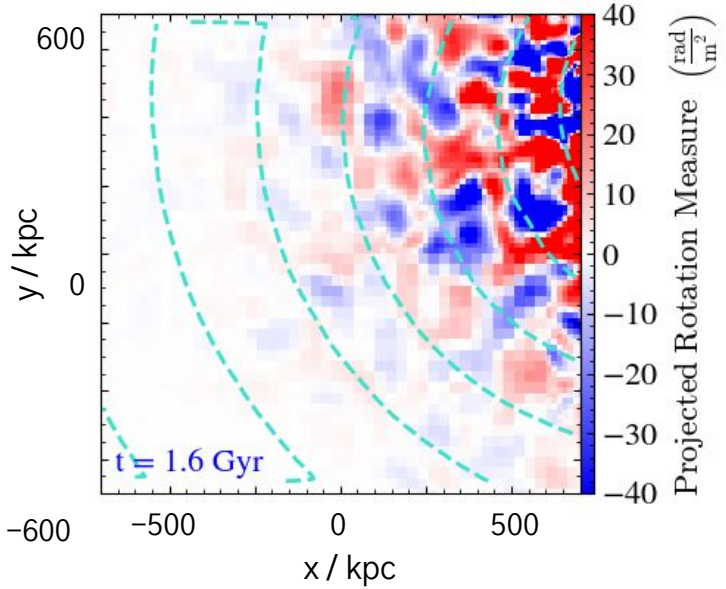

after

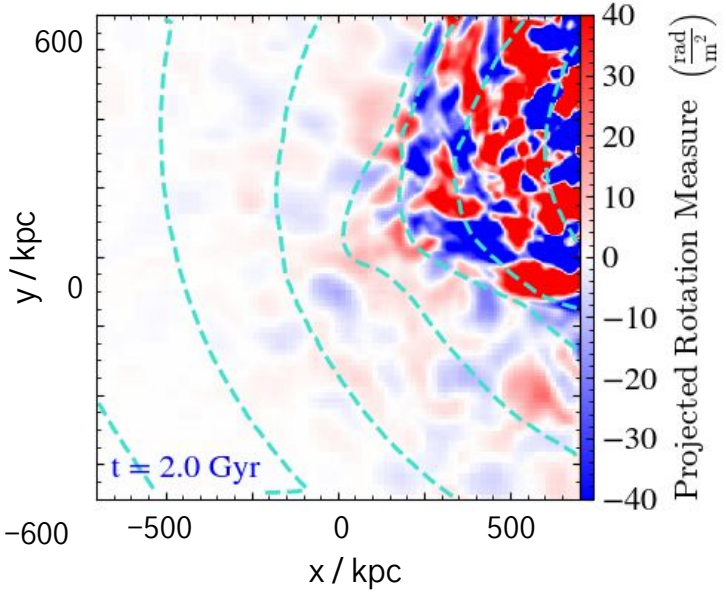

(Liou, **On,** Yang and ZuHone, ApJ, under review)

Comparing between the features in our simulation and the Fornax observations

POSSUM RM map

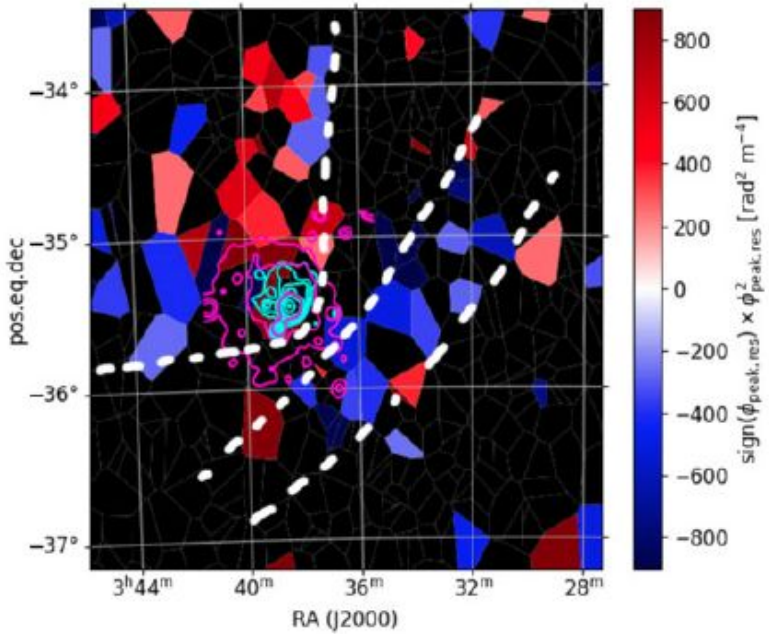

(Anderson+ 2021)

our simulated RM map

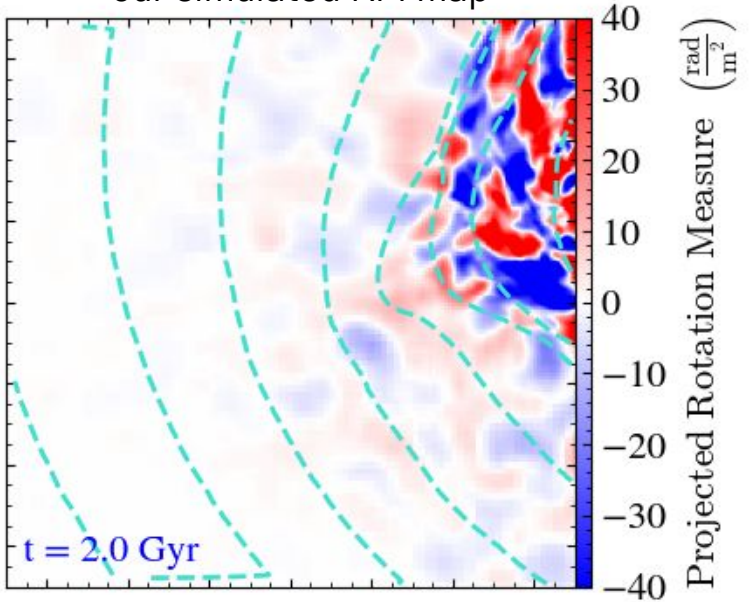

(Liou, **On,** Yang and ZuHone, ApJ, under review)

Decrease in RMs near the sloshing cold front

using 3D FLASH MHD simulations of a cluster merger scenario

colours: RM

cyan contours: projected X-ray emission

before

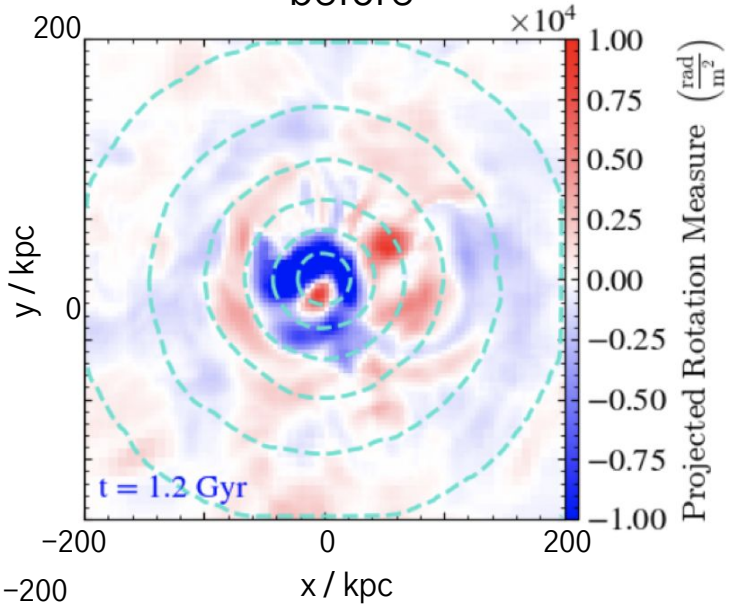

after

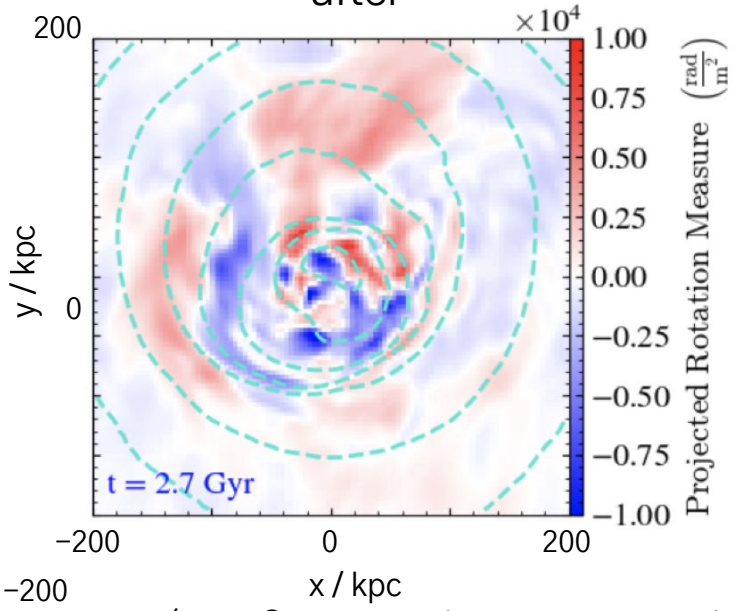

(Liou, **On,** Yang and ZuHone, ApJ, under review)

Comparing between the features in our simulation and the Fornax observations

POSSUM RM map

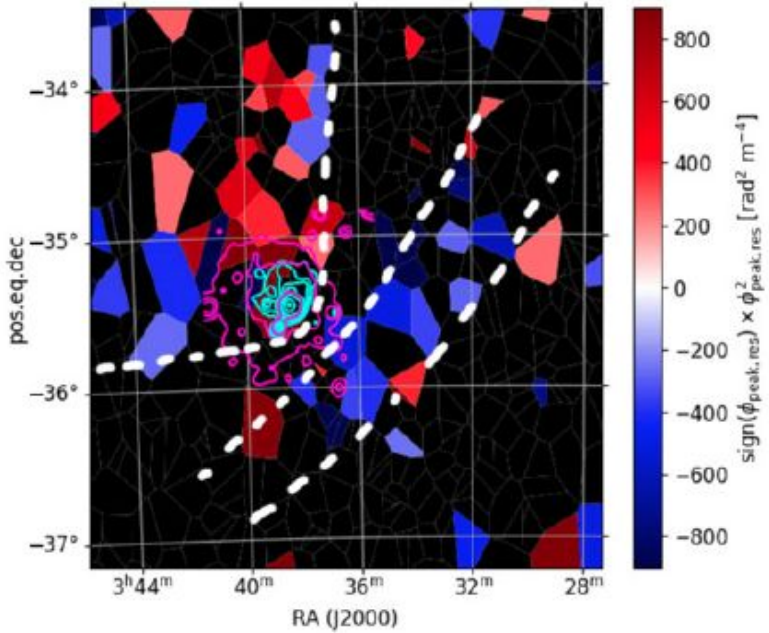

(Anderson+ 2021)

our simulated RM map

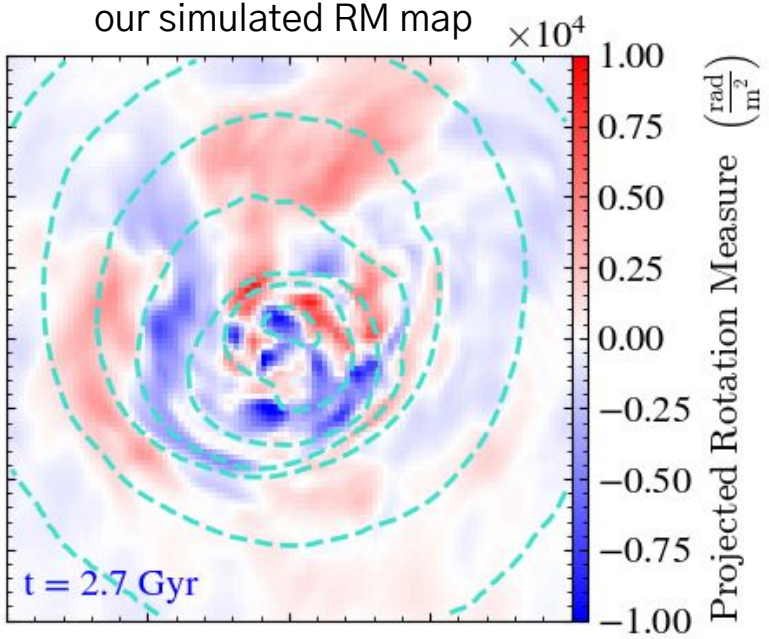

(Liou, **On,** Yang and ZuHone, ApJ, under review)

Summary

no clear explanation for the lack of polarised radio sources in the Fornax cluster

- faint sources are more easily depolarised or enhanced by the intracluster shock, whereas the polarisation of bright sources is largely unaffected
- enhanced local RMs behind the shock front on Mpc scales, due to the compression of hot gas and magnetic field lines
- decrease in RMs near the cluster center, as a result of field cancellations driven by sloshing turbulence

wishlist:

keep the (full) Stokes polarisations

search for any radio halo/relic in the Fornax cluster